

Optimization of the seismic processing phase-shift plus finite-difference migration operator based on a hybrid genetic and simulated annealing algorithm

Luo Renze^{1*}, Huang Yuanyi², Liang Xianghao³, Luo Jun⁴ and Cao Ying⁴

¹ State Key Laboratory of Oil and Gas Reservoir Geology and Exploitation, Southwest Petroleum University, Chengdu, Sichuan 610500, China

² Geophysics Development Department of BGP, Hebei 072751, China

³ Exploration and Exploitation Department of Tarim Oilfield Company, PetroChina, Korla, Xinjiang 418000, China

⁴ Changqing Oilfield Company, PetroChina, Ningxia 750000, China

© China University of Petroleum (Beijing) and Springer-Verlag Berlin Heidelberg 2013

Abstract: Although the phase-shift seismic processing method has characteristics of high accuracy, good stability, high efficiency, and high-dip imaging, it is not able to adapt to strong lateral velocity variation. To overcome this defect, a finite-difference method in the frequency-space domain is introduced in the migration process, because it can adapt to strong lateral velocity variation and the coefficient is optimized by a hybrid genetic and simulated annealing algorithm. The two measures improve the precision of the approximation dispersion equation. Thus, the imaging effect is improved for areas of high-dip structure and strong lateral velocity variation. The migration imaging of a 2-D SEG/EAGE salt dome model proves that a better imaging effect in these areas is achieved by optimized phase-shift migration operator plus a finite-difference method based on a hybrid genetic and simulated annealing algorithm. The method proposed in this paper is better than conventional methods in imaging of areas of high-dip angle and strong lateral velocity variation.

Key words: Migration operator, phase-shift plus finite-difference, hybrid algorithm, genetic and simulated annealing algorithm, optimization coefficient

1 Introduction

Currently, seismic exploration focuses on areas of complex structure and dramatic velocity variation. However, the conventional migration processing adopted in these areas cannot obtain precise imaging of the underground structure. Therefore, prestack depth migration is used instead, because it adapts well to the areas of complex structure and dramatic velocity variation and is one of the effective ways to image precisely (Zhu et al, 2010).

The core of prestack depth migration is the wave field propagation operator. The conventional methods to compute the wave field propagation operator are: the Kirchhoff integration based on a ray theory method (Keho and Beydoun, 1988), phase shift method (PS) (Gazdag, 1978), space-frequency domain finite difference method (FD) (Ma, 1983; Claerbout, 1985; Cheng et al, 2001), split step Fourier method (SSF) (Stoffa et al, 1990), Fourier finite difference method (FFD) (Ristow and Rühl, 1994) and the generalized screen propagator method (GSP) (Jin et al, 2002).

The phase shift method (PS) was first proposed by Gazdag (1978). This method has high accuracy, good stability, high efficiency, high-dip imaging and good adaptability to vertical velocity variation, but it is not able to adapt to strong lateral velocity variation. To overcome the defect of PS, Gazdag proposed the phase-shift wave equation migration plus interpolation method in 1984 (Gazdag and Sguazzero, 1984). Although the method improves PS to some extent, the computing workload increases dramatically.

On the basis of Gazdag's method, a phase-shift plus finite-difference migration method (PSFD) was proposed (Gazdag and Sguazzero, 1984), which retains PS's computing efficiency, zero frequency dispersion and good stability. In this method, a finite-difference method is adopted together with the phase-shift method. This adapts well to strong lateral velocity variation and avoids the defects of the pure phase-shift method. Besides PSFD, the other method (FFD) is adopted to add a finite difference adjustment of high accuracy on the basis of SSF, to enhance its ability to deal with strong lateral velocity variation and high-dip angle. This method integrates the strengths of both FD and PS. Therefore, it can tackle the problem of high-dip angle and strong velocity variation simultaneously with high precision (Zhang et al,

*Corresponding author. email: lrzsmith@126.com

Received June 18, 2012

2008). On the basis of phase-shift plus finite-difference, this paper proposes a method to optimize the coefficient of the single square root of the dispersion equation, increase approximation accuracy and, in the end, increase the imaging effect.

2 The process of coefficient optimization

The 2-D wave equation is written as:

$$\frac{\partial^2 u}{\partial x^2} + \frac{\partial^2 u}{\partial z^2} = \frac{1}{v^2} \frac{\partial^2 u}{\partial t^2} \tag{1}$$

where v stands for medium velocity, m/s; x and z are coordinate directions; $u(x, z, t)$ is seismic wave field; t is time, s.

Convert the above equation into a frequency-space domain equation by FFT:

$$\frac{\partial^2 u(x, z; \omega)}{\partial x^2} + \frac{\partial^2 u(x, z; \omega)}{\partial z^2} = \frac{\omega^2 u(x, z; \omega)}{v^2} \tag{2}$$

where $u(x, z; \omega)$ is the wave field of the frequency-space domain, ω is angle frequency (rad/s), and v is medium velocity.

The 2-D one-way equation in the frequency-space domain is written as:

$$\frac{\partial u(x, z; \omega)}{\partial z} = i \sqrt{\frac{\omega^2}{v^2} + \frac{\partial^2}{\partial x^2}} u(x, z; \omega) \tag{3}$$

where i is imaginary, $i = \sqrt{-1}$.

Converting Eq. (3) to a frequency-wave number domain equation by FFT:

$$\frac{\partial u(k_x, z; \omega)}{\partial z} = i \sqrt{\frac{\omega^2}{v^2} - k_x^2} u(k_x, z; \omega) \tag{4}$$

From Eq. (4), we derive the dispersion equation of a single square root operator:

$$k_z = \frac{\omega}{v} \sqrt{1 - \frac{v^2 k_x^2}{\omega^2}} \tag{5}$$

In Eqs. (4) and (5), k_x is the wave number of horizontal x ; k_z is the wave number of vertical z .

When the background velocity is $v_0(z)$, if $v_0(z)$ replaces medium velocity $v(x, z)$ in the single square root operator of the dispersion equation, the error is:

$$E = \sqrt{\frac{\omega^2}{v^2} - k_x^2} - \sqrt{\frac{\omega^2}{v_0^2} - k_x^2} = \frac{\omega}{v} \sqrt{1 - \frac{v^2}{\omega^2} k_x^2} - \frac{\omega}{v_0} \sqrt{1 - \frac{v_0^2}{\omega^2} k_x^2} \tag{6}$$

If $x = \frac{v^2}{\omega^2} k_x^2$, and $x \in (0, 1)$, then the square root in Eq. (6) is written as:

$$f(x) = \sqrt{1 - x} \tag{7}$$

The approximant of the first order to Eq. (7) is:

$$\sqrt{1 - x} \approx \frac{1 - ax}{1 - bx} \tag{8}$$

where a and b are the coefficients of the approximant.

Substituting Eq. (8) into Eq. (6), the following equation is derived:

$$E \approx \frac{\omega}{v} \left[\frac{1 - a \left(\frac{v}{\omega} k_x \right)^2}{1 - b \left(\frac{v}{\omega} k_x \right)^2} \right] - \frac{\omega}{v_0} \left[\frac{1 - a \left(\frac{v_0}{\omega} k_x \right)^2}{1 - b \left(\frac{v_0}{\omega} k_x \right)^2} \right] \tag{9}$$

Convert Eq. (9) to frequency-space domain:

$$E \approx \frac{\omega}{v} \left[\frac{1 + a \left(\frac{v^2}{\omega^2} \frac{\partial^2}{\partial x^2} \right)}{1 + b \left(\frac{v^2}{\omega^2} \frac{\partial^2}{\partial x^2} \right)} \right] - \frac{\omega}{v_0} \left[\frac{1 + a \left(\frac{v_0^2}{\omega^2} \frac{\partial^2}{\partial x^2} \right)}{1 + b \left(\frac{v_0^2}{\omega^2} \frac{\partial^2}{\partial x^2} \right)} \right]$$

$$= \left(\frac{\omega}{v} - \frac{\omega}{v_0} \right) + \frac{\omega}{v} \left[\frac{(a - b) \frac{v^2}{\omega^2} \frac{\partial^2}{\partial x^2}}{1 + b \left(\frac{v^2}{\omega^2} \frac{\partial^2}{\partial x^2} \right)} \right] - \frac{\omega}{v_0} \left[\frac{(a - b) \frac{v_0^2}{\omega^2} \frac{\partial^2}{\partial x^2}}{1 + b \left(\frac{v_0^2}{\omega^2} \frac{\partial^2}{\partial x^2} \right)} \right] \tag{10}$$

The depth propagation equation of the wave field is:

$$u(x, z_i + \Delta z; \omega) = u(x, z_i; \omega) e^{ik_z \Delta z} = u(x, z_i; \omega) e^{i \left(\sqrt{\frac{\omega^2}{v_0^2} + \frac{\partial^2}{\partial x^2} + E} \right) \Delta z} \tag{11}$$

Thus, k_z in Eq. (11) is written as:

$$k_z \approx \sqrt{\frac{\omega^2}{v_0^2} + \frac{\partial^2}{\partial x^2}} + \left(\frac{\omega}{v} - \frac{\omega}{v_0} \right) + \frac{\omega}{v} \left[\frac{(a - b) \frac{v^2}{\omega^2} \frac{\partial^2}{\partial x^2}}{1 + b \left(\frac{v^2}{\omega^2} \frac{\partial^2}{\partial x^2} \right)} \right]$$

$$- \frac{\omega}{v_0} \left[\frac{(a - b) \frac{v_0^2}{\omega^2} \frac{\partial^2}{\partial x^2}}{1 + b \left(\frac{v_0^2}{\omega^2} \frac{\partial^2}{\partial x^2} \right)} \right] \tag{12}$$

where the first factor is the constant velocity phase-shift operator in the frequency-wave number domain; the second factor is the adjusted time-shift operator in the frequency-space domain; the third and fourth factors are the frequency-space difference operators in the disturbance wave field.

A higher precision will be obtained if a higher-order approximation is adopted in Eq. (8) at the cost of greatly increased computation. Usually the optimized coefficient can both increase the accuracy of the algorithm and maintain the same order as well as computing efficiency. As a result, it is more widely adopted in practice. Xie and Wu (1999) improved the high-dip imaging of FFD by optimizing the FFD operator of the Padé expansion. Nevertheless, the numerator and denominator of the Padé expansion are determined by the formal power series expansion of the approximating function, which although reveals as much information about the approximating function as possible, its vertex position is hard to control (Zhang and Zhao, 2010). Huang and Fehler (2000) proposed a globalized scheme of adopting only one series of optimized coefficients to adapt to various velocity variations. Fu et al (2007) proposed a degenerate Fourier migration operator by approximating the degenerate kernel of the Lippmann-Schwinger one-way wave integral equation. But this method employs a Taylor expansion and a rational approximation splitting algorithm, both of whose approximating effects are not ideal. Zhu et al (2008) achieved higher precision globalized coefficients by simulated annealing, which has to be completed within limited time and has to adjust parameters for different situations. Therefore, an improved simulated annealing, i.e. genetic and simulated annealing, is adopted in this paper. Zhang and Yao (2011) also applied the globalized optimization in a 3-D splitting error amendment.

3 The computation and performance analysis of optimized coefficients

To compute the third and fourth factors in Eq. (12), a genetic and simulated annealing hybrid algorithm was employed (Zhang and Wang, 2011). The simulated annealing algorithm can be iterated and adjusted, within certain possibilities, to the degrading of the target function. Local optimum points in the optimization process can thus be avoided and globalized optimum analytic solutions can be guaranteed. However, this method is very slow to converge. Though the genetic algorithm is able to obtain the globalized optimum solutions with higher probability and has a feature of implicit parallel arithmetic, it has the defect of immature convergence. To avoid the above-mentioned defects, the hybrid genetic and simulated annealing algorithm is adopted in this paper. This algorithm has advantages over pure genetic or simulated annealing algorithm in the following aspects (Zhang and Wang, 2011): improvement of optimum performance, increase of optimization efficiency, and increase of robustness.

If the incidence angle is θ and $\sin(\theta) = \frac{vk_x}{\omega}$, Eq. (8) is written as:

$$\sqrt{1 - \sin^2(\theta)} = \frac{1 - a \sin^2(\theta)}{1 - b \sin^2(\theta)} \tag{13}$$

$$\min f = \frac{1 - a \sin^2(\theta)}{1 - b \sin^2(\theta)} \approx 0 \tag{14}$$

The coefficient of Eq. (14) is computed by the hybrid genetic and simulated annealing algorithm. The initial parameters are given as: initial temperature $c_0=200$ °C $\theta_{max}=85^\circ$, and the optimized coefficients $a=0.8752$, $b=0.3896$. Eq. (12) is written as:

$$k_z \approx \sqrt{\frac{\omega^2}{v_0^2} + \frac{\partial^2}{\partial x^2}} + \left(\frac{\omega}{v} - \frac{\omega}{v_0}\right) + \frac{\omega}{v} \left[\frac{0.4856 \frac{v^2}{\omega^2} \frac{\partial^2}{\partial x^2}}{1 + 0.3896 \left(\frac{v^2}{\omega^2} \frac{\partial^2}{\partial x^2}\right)} \right] - \frac{\omega}{v_0} \left[\frac{0.4856 \frac{v_0^2}{\omega^2} \frac{\partial^2}{\partial x^2}}{1 + 0.3896 \left(\frac{v_0^2}{\omega^2} \frac{\partial^2}{\partial x^2}\right)} \right] \tag{15}$$

The relative error between the approximant with optimized coefficients and the precise dispersion equation is:

$$E_r(\theta) = \frac{1 - 0.8752 \sin^2(\theta)}{1 - 0.3896 \sin^2(\theta)} - \cos(\theta) \tag{16}$$

Comparing our error with the previous relative error between the approximant with coefficients of $a=0.8528$, $b=0.3767$ and the precise dispersion equation, we obtain error curves as illustrated in Fig. 1. Fig. 1 shows that the error curve of optimized coefficients is lower than that of the previous coefficients. Therefore, the approximant achieves better effects with optimized coefficients.

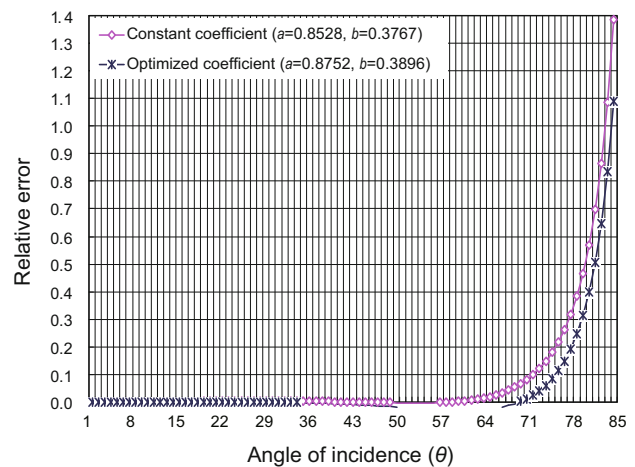


Fig. 1 Curve charts of the relative errors between approximations of different coefficients and precise value

To better compare the approximation effects between the optimized coefficients $a=0.8752$, $b=0.3896$ and the existing coefficients $a=0.8528$, $b=0.3767$, we calculate their respective mathematic expectations of the relative errors between them and the precise values.

$$E = \frac{\sum_{k=0}^n |E_r(\theta)|}{n} \tag{17}$$

The mathematic expectation of the relative error between the optimized coefficients $a=0.8752$, $b=0.3896$ and the precise value is $E=0.062681$, and the mathematic expectation between the existing coefficients $a=0.8528$, $b=0.3767$ and the precise value is $E=0.085439$. On the basis of the above comparison, we arrive at the conclusion that the optimized coefficients proposed in this paper can achieve much better approximation precision and smaller relative errors.

4 Simulated imaging by an optimized coefficient migration operator

To test the performance of the method proposed in this paper—the phase-shift plus finite-difference migration operator on the basis of hybrid genetic and simulated annealing algorithm, we conducted prestack depth migration imaging for a 2-D SEG/EAGE salt dome model with the optimized operator.

2-D SEG/EAGE salt dome models have complex geologic features, complicated structures and dramatic lateral velocity variation. In particular, the high-velocity salt dome in the center makes imaging difficult. The velocity field parameters of the model are: 1,290 (lateral sampling), 300 (vertical sampling), 12 m (lateral sampling interval), and 12 m (vertical sampling interval). The model is illustrated in Fig. 2.

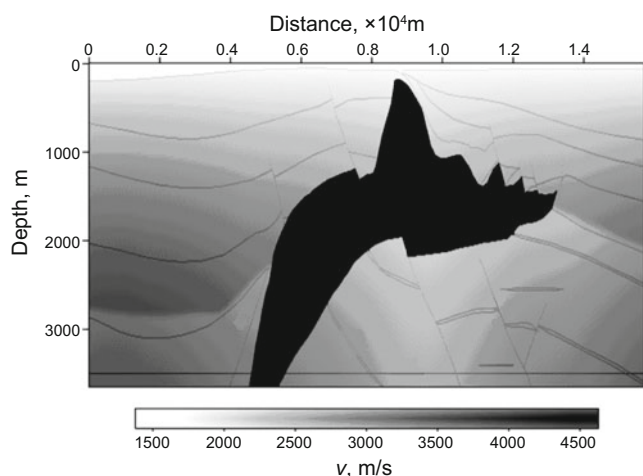


Fig. 2 Velocity model of a 2-D SEG/EAGE salt dome

For a 2-D SEG/EAGE salt dome, two prestack depth migrations are conducted with phase-shift plus finite-difference migration operator of conventional coefficients and phase-shift plus finite-difference migration operator of optimized coefficients. The profiles of the two migrations are demonstrated in Figs. 3 and 4 respectively.

Comparing the profiles in Figs. 3 and 4, we arrive at the conclusion that the imaging effect in Fig. 4 is better than that in Fig. 3, with a clearer salt dome structure, more clear-cut structure boundaries, and a much more distinct wave field below the salt dome. Therefore, a phase-shift plus finite-difference migration operator based on hybrid genetic and simulated annealing algorithm achieves better imaging than a phase-shift plus finite-difference migration operator of conventional coefficients. Therefore, the new method

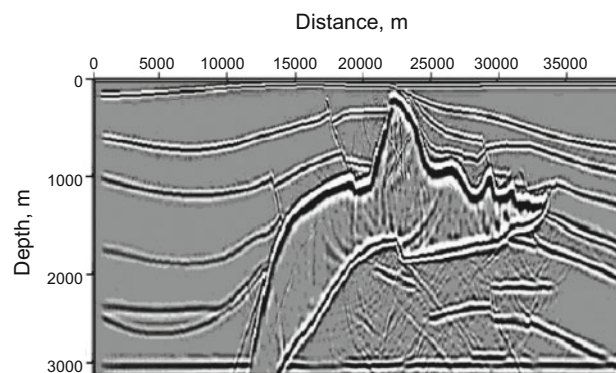


Fig. 3 Prestack depth migration profile of the 2-D SEG/EAGE salt dome model by phase-shift plus finite-difference of constant coefficients

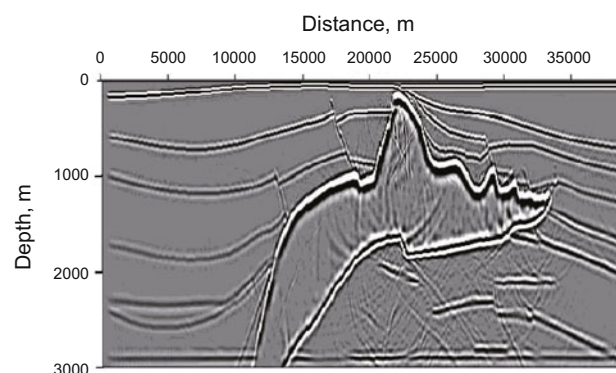


Fig. 4 Prestack depth migration profile of the 2-D SEG/EAGE salt dome model by an optimized phase-shift plus finite-difference operator of hybrid genetic and simulated annealing algorithm

proposed in this paper adapts better to areas with strong lateral velocity variation.

5 Conclusions

Compared with conventional coefficients, the optimized coefficients achieve better imaging. The key is that the approximation by the hybrid algorithm can better approximate the precise single square root dispersion equation. Consequently, the descriptive accuracy of strong lateral velocity variation medium is improved. In conclusion, phase-shift plus finite-difference migration operator of optimized coefficients based on a hybrid genetic and simulated annealing algorithm can attain better imaging in areas of high-dip angle and strong lateral velocity variation.

Acknowledgements

The authors would like to thank the Open Fund (PLC201104) of State Key Laboratory of Oil and Gas Reservoir Geology and Exploitation (Chengdu University of Technology), the National Natural Science Foundation of China (No.61072073) and the Key Project of Education Commission of Sichuan Province (No.10ZA072).

References

Cheng J B, Wang H Z and Ma Z T. Pre-stack depth migration with finite-

- difference method in frequency-space domain. *Chinese Journal of Geophysics*. 2001. 44(3): 389-395 (in Chinese)
- Claerbout J F. *Imaging the Earth's Interior*. USA: Blackwell Scientific Publications. 1985
- Fu L Y, Sun W J and Li D P. Degenerate migrators for imaging fault-related complex structures. *Chinese Journal of Geophysics*. 2007. 50(4): 1241-1250 (in Chinese)
- Gazdag J. Wave equation migration with the phase-shift method. *Geophysics*. 1978. 7: 1342-1351
- Gazdag J and Sguazzero P. Migration of seismic data by phase shift plus interpolation. *Geophysics*. 1984. 49(2): 124-131
- Huang L J and Fehler M C. Globally optimized Fourier finite-difference migration method. 70th Annual International Meeting, SEG. 2000. 802-805
- Jin S W, Xu S Y and Wu R S. Wave equation based prestack depth migration using generalized screen propagation. *Chinese Journal of Geophysics*. 2002. 45(5): 684-690 (in Chinese)
- Keho T H and Beydoun W B. Paraxial ray Kirchhoff migration. *Geophysics*. 1988. 53(12): 1540-1546
- Ma Z T. Splitting algorithm on higher order wave equation migration. *Acta Geophysica Sinica*. 1983. 26(4): 377-388
- Ristow D and Rühl T. Fourier finite-difference migration. *Geophysics*. 1994. 59(12): 1882-1893
- Stoffa P L, Fokkema J T, de Luna Freire R M, et al. Split-step Fourier migration. *Geophysics*. 1990. 55(4): 410-421
- Xie X B and Wu R S. Improving the wide angle accuracy of the screen propagator for elastic wave propagation. 69th Annual International Meeting, SEG. 1999. 1863-1866
- Zhang J H, Wang W M, Fu L Y, et al. 3D Fourier finite-difference migration by ADI plus interpolation. *Geophysical Prospecting*. 2008. 56: 95-103
- Zhang J H and Yao Z X. Reducing two-way splitting error of FFD method in dual domains. *Geophysics*. 2011. 76(4): S165-S175
- Zhang J M and Wang H L. B-spline curve fitting based on genetic algorithms and the simulated annealing algorithm. *Computer Engineering & Science*. 2011. 33(3): 191-193 (in Chinese)
- Zhang N and Zhao Q J. Generalized Lagrange blending rational interpolation based on the Padé approximation. *Journal of Anhui University of Science and Technology*. 2010. 30(1): 68-72 (in Chinese)
- Zhu J, Mathewson J and Liebelt G. A case study for azimuthally anisotropic prestack depth imaging of an onshore Alaska prospect. *Geophysics*. 2010. 75(4): 177-186
- Zhu S W, Zhang J H and Yao Z X. Globally optimized Fourier finite-difference operator using simulated annealing algorithm based on multi-parameter. *Chinese Journal of Geophysics*. 2008. 51(6): 1844-1850 (in Chinese)

(Edited by Hao Jie)